Contribution from the Department of Chemistry, Willard H. Dow Laboratory, University of Michigan, Ann Arbor, Michigan 48109-1055

Modeling Vanadium Bromoperoxidase: Synthesis, Structure, and Spectral Properties of Vanadium(IV) Complexes with Coordinated Imidazole

Charles R. Cornman, Jeff Kampf, Myoung Soo Lah, and Vincent L. Pecoraro*

Received September 16, 1991

A series of vanadium(IV)-SALIMH complexes [HSALIMH = 4-(2-(salicylideneamino)ethyl)imidazole] have been synthesized and characterized by X-ray crystallography, electron paramagnetic resonance, infrared, and visible spectroscopy, and mass spectrometry. The compounds VO(SALIMH)ACAC·MeOH (**1**), VO(SALIMH)SAL·MeOH (SAL is the anion of salicylaldehyde) (**2**), and $VO(SALIMH)_2 \cdot 3EtOH$ (**3**) represent the first fully characterized vanadium(IV) compounds with imidazole in their coordination sphere. Compounds **1-3** react reversibly with acid to form complexes in which either the bound imidazole has been protonated (**1'** and **3'**) or the bidentate ligand has been protonated and subsequently displaced by solvent (**4**). Addition of excess acid yields the solvated vanadyl ion $VO(SOL)_5^{2+}$ (**5**) (SOL = solvent). Protonation and subsequent ligand displacement by solvent induce an increase in the EPR hyperfine coupling constants $A_\parallel$ and $A_\perp$. The implications of this work toward understanding the reduced catalytically inactive form of vanadium bromoperoxidase are discussed. X-ray parameters are as follows: **1**, $C_{18}H_{23}N_3O_5V_1$, 412.34 g/mol, crystal system, orthorhombic (*Pbca*), a = 20.673 (4) Å, b = 21.335 (4) Å, c = 9.078 (1) Å, V = 4404 (1) Å^3, Z = 8, 2629 data collected with $5° < 2\theta < 45°$, 1807 data collected with $F_o > 6\sigma(F)$, R = 0.039, R_w = 0.038; **2**, $C_{20}H_{21}N_3O_5V_1$, 434.34 g/mol, crystal system, orthorhombic (*Pbca*), a = 12.336 (5) Å, b = 14.928 (6) Å, c = 22.03 (1) Å, V = 4067 (3) Å^3, Z = 8, 3588 data collected with $5° < 2\theta < 50°$, 2723 data collected with $F_o > 2.0\sigma(F)$, R = 0.0799, R_w = 0.0479; **3**, $C_{30}H_{42}N_6O_6V_1$, 633.64 g/mol, crystal system, monoclinic ($P2_1/c$), a = 13.763 (7) Å, b = 17.589 (4) Å, c = 14.701 (2) Å, β = 108.97 (2)°, V = 3365 (1) Å^3, Z = 4, 4398 data collected with $5° < 2\theta < 45°$, 3059 data collected with $F_o > 5\sigma(F)$, R = 0.0697, R_w = 0.0949.

Introduction

Little is known about the coordination chemistry of vanadium in biological systems.[1] The complex amavadin from the mushroom *Amanita muscaria* was isolated and characterized in 1973, and while the function of this compound remains unknown, amavadin represents the first example of a vanadium coordination complex from a biological source that has been defined fully.[2] In the mid-1980s, two enzymes dependent on vanadium for activity were identified and characterized. A vanadium nitrogenase, which catalyzes the reduction of dinitrogen to ammonia, has been isolated from several species of *Azotobacter*.[3] Vanadium-dependent bromoperoxidase[4] (V-BrPO) has been isolated from several marine algae[5] and a terrestrial lichen.[6] Vanadium bromoperoxidase catalyzes the peroxide-dependent halogenation of organic compounds in the presence of halide ion as in eq 1. The importance

$$RH_2 + H_2O_2 + H^+ + Br^- \xrightarrow{\text{V-BrPO}} RHBr + 2H_2O \quad (1)$$

of vanadium in both reductive (nitrogenase) and oxidative (peroxidase) catalytic transformations exemplifies the versatility of the vanadium ion in biological chemistry and has stimulated our interest in the coordination and reaction chemistry of this element. In particular, we have focused our attention on modeling the novel structure, spectroscopy, and reactivity of vanadium bromoperoxidase.

The literature concerning vanadium bromoperoxidases has recently been reviewed.[1] Kinetic studies on the native enzyme[7] are consistent with an ordered two-substrate mechanism in which hydrogen peroxide and halide ion sequentially bind to the active site to generate the reactive halogenating intermediate. The exact composition of the active oxidant and the active halogenating intermediate is not known. V-BrPO has been shown to function as a chloroperoxidase as well as a bromo- and iodoperoxidase.[8] In the absence of organic substrate, vanadium bromoperoxidase has catalase activity.[9] The vanadium ion in V-BrPO is not coordinated by a porphyrin and is believed to be in the +5 oxidation state.[10] Two metal binding sites, one weak and inactive and one stronger and active, have been observed by ^{51}V NMR.[11] EXAFS measurements[12] on the vanadium(V) form of the enzyme suggest that the vanadium is coordinated by six or seven oxygen/nitrogen ligands. One of the light atoms is at ≈1.6 Å, which is consistent with a vanadium-oxo unit. A second shell at ≈1.7 Å is suggestive of a vanadate ester oxygen. The other ligand heteroatoms are each at a distance of approximately 2 Å. V-BrPO has a ^{51}V NMR shift of −1250 ppm.[13] On the basis of the shifts of model vanadium(V) complexes, it has been proposed that the vanadium ion is high coordinate and the coordination sphere is rich in oxygen, probably from η^2-carboxylate functional groups.[14] EXAFS results for the dithionite-reduced enzyme have been modeled by a short V=O distance of ≈1.6 Å, two or three nitrogen/oxygen ligands at ≈1.90 Å, and two light atoms at ≈2.05 Å. Second shell modeling is suggestive of imidazole coordination.

(1) For recent reviews of biologically relevant vanadium chemistry, see: (a) *Vanadium in Biological Systems*; Chasteen, N. D., Ed.; Kluwer Academic Publishers: Dordrecht, The Netherlands, 1990. (b) Butler, A.; Carrano, C. J. *Coord. Chem. Rev.* **1991**, *109*, 61. (c) Rehder, D. *Angew. Chem., Int. Ed. Engl.* **1991**, *30*, 148.

(2) (a) Kneifel, H.; Bayer, E. *Angew. Chem., Int. Ed. Engl.* **1973**, *12*, 508. (b) de C. T. Carrondo, M. A. A. F.; Duarte, M. T. L. S.; Pessoa, J. C.; Silva, J. A. L.; Frausto da Silva, J. J. R.; Vaz, M. C. T. A.; Vilas-Boas, L. F. *J. Chem. Soc., Chem. Commun.* **1988**, 1158. (c) Armstrong, E. M.; Calviou, L. J.; Charnock, J. M.; Collison, D.; Ertok, N.; Garner, C. D.; Mabbs, F. E.; Naismith, J. H. Abstract—Fifth International Conference on Bioinorganic Chemistry. *J. Inorg. Biochem.* **1991**, *43*, 413.

(3) (a) Robson, R. L.; Eady, R. R.; Richardson, T. H.; Miller, R. W.; Hawkins, M.; Postgate, J. R. *Nature* **1986**, *322*, 388. (b) Hales, B. J.; Case, E. P.; Morningstar, J. E.; Dzeda, M. F.; Mauterer, L. A. *Biochemistry* **1986**, *25*, 7251.

(4) Recent work by Butler et al.[8] demonstrating chloroperoxidase activity may necessitate use of the general term "haloperoxidase" to describe this system.

(5) (a) Vilter, H. *Bot. Mar.* **1983**, *26*, 429. (b) Vilter, H. *Bot. Mar.* **1983**, *26*, 451. (c) de Boer, E.; Tromp, M. G. M.; Plat, H.; Krenn, B. E.; Wever, R. *Biochim. Biophys. Acta* **1986**, *872*, 104. (d) Soedjak, H. S.; Butler, A. *Biochemistry* **1990**, *29*, 7974.

(6) Plat, H.; Krenn, B. E.; Wever, R. *Biochem. J.* **1987**, *248*, 277.

(7) (a) de Boer, E.; Wever, R. *J. Biol. Chem.* **1988**, *263*, 12326. (b) Soedjak, H. S.; Butler, A. *Biochim. Biophys. Acta* **1991**, *1079*, 1.

(8) Soedjak, H. S.; Butler, A. *Inorg. Chem.* **1990**, *29*, 5015.

(9) Everett, R. R.; Butler, A. *Inorg. Chem.* **1989**, *28*, 393.

(10) Wever, R.; Kren, B. E. In *Vanadium in Biological Systems*; Chasteen, N. D., Ed.; Kluwer Academic Publishers: Dordrecht, The Netherlands, 1990; pp 81-97.

(11) Rehder, D.; Holst, H.; Preibsch, W.; Vilter, H. *J. Inorg. Biochem.* **1991**, *41*, 171.

(12) Arbor, J. M.; de Boer, E.; Garner, C. D.; Hasnain, S. S.; Wever, R. *Biochemistry* **1989**, *28*, 7968.

(13) (a) Vilter, H.; Rehder, D. *Inorg. Chim. Acta* **1987**, *136*, L7. (b) Rehder, D.; Vilter, H.; Duch, A.; Preibsch, W.; Weidemann, C. *Recl. Trav. Chim. Pays-Bas* **1987**, *106*, 408.

(14) Rehder, D.; Weidemann, C.; Duch, A.; Priebsch, W. *Inorg. Chem.* **1988**, *27*, 584.

0020-1669/92/1331-2035$03.00/0

Additional evidence supporting the presence of imidazole at the active site of V-BrPO has been provided by several techniques. EPR measurements on the dithionite-reduced enzyme[15] yield axial spectra typical for five- and six-coordinate vanadyl (V^{IV}=O) complexes which have a distribution of oxygen and nitrogen donors in their coordination sphere.[16] The EPR spectrum is pH dependent and suggests the presence of an ionizable residue near the vanadium ion with a pK_a = 5.4. Most strikingly, electron spin-echo envelope modulation (ESEEM) experiments indicate the presence of nitrogen (imidazole) in the vanadium coordination sphere.[17]

Solution studies of aqueous vanadate–imidazole systems are indicative of a vanadate–imidazole interaction. Dlouhá and coworkers have shown that vanadate-induced oxidation of NADH is inhibited in imidazole (and histidine) buffer.[18] Crans et al. have shown that imidazole buffer can affect both the equilibria and kinetics of vanadate reactions in aqueous solution.[19] While imidazole mimetic ligands with amino,[20,21] imino,[21,22] or pyrazolyl[23] functional groups have been utilized to study vanadium–nitrogen interactions, there is only one structurally characterized vanadium(IV) coordination compound reported with imidazole coordinated to the metal center.[24] This crystallographic report does not describe any of the solution spectroscopy or chemistry of the vanadium(IV)–imidazole complex. This contribution details the synthesis and structural characterization of three vanadium(IV)–imidazole coordination complexes. The structural characterization of a vanadium(V)–imidazole complex will be reported separately.[25] The acid/base chemistry and spectral properties of these important compounds are also reported and compared to the properties of the reduced vanadium bromoperoxidase.

Experimental Section

Materials. Reagents were purchased from Aldrich Chemicals Inc. and used as received unless otherwise noted. Absolute ethanol was purchased from Midwest Grain Products Co. Abbreviations used: HSALIMH = 4-(2-(salicylideneamino)ethyl)imidazole; HACAC = 2,4-pentanedione; HSAL = salicylaldehyde.

Triethyl Vanadate. The triethyl ester of vanadic acid, $VO(OEt)_3$, was prepared by a modified literature procedure.[26] In a typical preparation, V_2O_5 was refluxed in absolute ethanol overnight. The resulting green slurry was filtered through a tared fritted funnel to yield a clear, pale yellow filtrate. The precipitate was dried under nitrogen and the mass was determined. On the assumption that the residual solid was unreacted V_2O_5, the amount of dissolved vanadic acid ester, $VO(OEt)_3$, was calculated. Typically, 10 wt % of vanadium oxide remained unreacted. The vanadate ester was never isolated.

4-(2-(Salicylideneamino)ethyl)imidazole. HSALIMH was prepared by mixing histamine dihydrochloride (1 equiv), salicylaldehyde (1 equiv), and sodium hydroxide (2 equiv) in 100 mL of absolute ethanol or methanol. The solution was refluxed for 20 min, cooled to room temperature, and filtered through a glass frit. Typically, vanadium salts were added directly to the ligand reaction mixture without further ligand purification. Analytically pure HSALIMH can be isolated by removing the alcohol solvent under vacuum, redissolving the yellow oil in chloroform, filtering through a glass frit to remove NaCl, and evaporating the filtrate under vacuum at elevated temperature (≈40 °C) for 12 h to yield a viscous yellow oil (usually ≥90%). ^{1}H NMR in $CDCl_3$, δ (ppm), multiplicity, integration: 13.09, s, 2 H; 8.18, s, 1 H; 7.61, s, 1 H; 7.2, m, 2 H; 6.84, m, 3 H; 3.82, t, 2 H; 2.92, t, 2 H. ^{13}C NMR in $CDCl_3$, δ (ppm): 165.22, 161.43, 134.55, 134.41, 132.24, 131.23, 118.49, 118.31, 117.03, 116.91, 58.47, 28.32. High-resolution mass spectrum: calculated for $C_{12}H_{13}N_3O$ = 215.1059; found = 215.1055. UV–vis in methanol solution [wavelength, nm (ε, M^{-1} cm^{-1})]: 402 (1150), 314 (3010), 254 (9420), 214 (23200). Important IR vibrations (from oil on NaCl plates) in cm^{-1}: 2916, 2849, 2734, 1632, 1581, 1492, 1457, 1279, 950, 756.

(Acetylacetonato)[4-(2-(salicylideneamino)ethyl)imidazolyl]oxovanadium(IV)·CH_3OH [VO(SALIMH)ACAC·CH_3OH, 1]. To a methanol (150-mL) solution of 19.1 mmol of HSALIMH (prepared as above) was added 18.9 mmol of vanadyl acetylacetonate (5.00 g, approximately 1 equiv). The solution was refluxed for 30 min and cooled to room temperature. The red-brown, X-ray-quality crystals which formed upon slow evaporation were collected and dried under vacuum to yield 5.11 g (65%). Anal. Calcd for $C_{18}H_{23}N_3O_5V$: C, 52.43; H, 5.62; N, 10.19; V, 12.36. Found: C, 52.76; H, 5.61; N, 10.29; V, 12.28. Important IR bands (cm^{-1}): 3152, 3122, 3050, 2925, 1634, 1600, 1514, 1471, 1449, 1395, 1028, 945, 764, 624.

[4-(2-(Salicylideneamino)ethyl)imidazolyl](salicylaldehydato)oxovanadium(IV) [VO(SALIMH)SAL, 2]. To a solution of 5.58 mmol of HSALIMH in 125 mL of MeOH was added 2.79 mmol of vanadyl sulfate (assuming the trihydrate, 0.605 g). The reaction mixture was refluxed overnight (ca. 12 h), cooled to room temperature, and filtered through a glass frit to yield a brown solution and a white solid. The filtrate was concentrated under vacuum to yield more white precipitate which was removed by filtration and discarded. The solution was then diluted with an equal volume of water, and the methanol was removed under vacuum to yield a red powder which was collected by filtration. Brick red microcrystals were obtained by slow evaporation of a methanol solution of the red powder, yield 0.639 g (53%). X-ray-quality crystals of **2** were obtained from a methanol solution of the crude reaction mixture (in the presence of excess sodium methoxide) which was kept at −20 °C for several days. Anal. Calcd for $C_{20}H_{21}N_3O_5V$: C, 55.31; H, 4.87; N, 9.67; V, 11.73. Found: C, 55.33; H, 4.72; N, 9.86; V, 12.23. Important IR bands (cm^{-1}): 3480, 2922, 2853, 1634, 1625, 1528, 1446, 1306, 1150, 956, 949, 903, 761, 603.

Bis[4-(2-(salicylideneamino)ethyl)imidazolyl]oxovanadium(IV)·EtOH [VO(SALIMH)$_2$·EtOH, 3]. To a refluxing ethanol solution of $VO(OEt)_3$ (0.6080 g of V_2O_5, 150 mL of ethanol (absolute), 0.0757 g of residue, 5.85 mmol of $VO(OEt)_3$) was added 17.5 mmol of HSALIMH in 100 mL of ethanol (absolute). The solution was refluxed approximately 20 h. The resulting deep brown solution was concentrated under vacuum to approximately 100 mL and allowed to stand overnight to yield 2.34 g (81%) of brown crystals. X-ray-quality crystals of the trisolvate were obtained by letting the capped reaction mixture sit undisturbed overnight. Anal. Calcd for $C_{26}H_{30}N_6O_4V$: C, 57.67; H, 5.58; N, 15.52; V, 9.41. Found: C, 57.48; H, 5.56; N, 15.48; V, 9.40. Important IR bands (cm^{-1}): 3099, 3042, 3020, 2967, 2915, 2866, 2748, 2651, 1616, 1596, 1472, 1448, 1403, 1313, 1297, 1151, 941, 910, 761.

Physical Measurements. (A) X-ray Crystallography. Single crystals of **1-3** were acquired as described above and mounted in sealed glass capillaries. A small amount of mother liquid was included in the capillary of **3** to decrease decomposition due to solvent loss from the crystal lattice. Diffraction data were collected on a Siemens R3m/v diffractometer (four-circle geometry) at ambient temperature. Intensity data were obtained using Mo Kα radiation (0.7107 Å) monochromatized from a graphite crystal whose diffraction vector was parallel to the diffraction vector of the sample. Three standard reflections were measured every 97 reflections. For compounds **1** and **2**, random fluctuations of less than 3% were observed for the three standard reflections. Standard reflections for **3** decayed ca. 8% over the course of the data collection, and a linear correction was applied. No absorption corrections were applied. Lattice parameters were determined from a least squares refinement of 15 reflection settings obtained from an automatic centering routine. Table I contains a summary of data collection conditions and results for each structure. The data were reduced and the structures were solved by direct methods using the program SHELXTL PLUS mounted on a VAXStation 3500. In subsequent refinement, the function $\sum w(|F_o| - |F_c|)^2$ was minimized, where $|F_o|$ and $|F_c|$ are the observed and calculated structure factor amplitudes. The agreement indices $R = \sum(|F_o| - |F_c|)/\sum|F_o|$ and $R_w = [\sum(|F_o| - |F_c|)^2/\sum w|F_o|^2]^{1/2}$ were used to evaluate the results. Atomic scattering factors are from the *International Tables for X-ray Crystallography*.[27] Hydrogen atoms were included using a riding model (d_{C-H} = 0.96 Å, isotropic U(H) fixed at 0.07 for **1** and refined to 0.066

(15) de Boer, E.; Boon, K.; Wever, R. *Biochemistry* **1988**, *27*, 1629.
(16) Chasteen, N. D. In *Biological Magnetic Resonance*; Berliner, L. J., Reuben, J., Eds.; Plenum Press: New York, 1981; Vol. 3, pp 53–119.
(17) de Boer, E.; Keijzers, C. P.; Klaassen, A. A. K.; Reijerse, E. J.; Collison, D.; Garner, C. D.; Wever, R. *FEBS Lett.* **1988**, *235*, 93.
(18) Vyskocil, F.; Teisinger, J.; Dlouhá, H. *Nature* **1980**, *286*, 516.
(19) Crans, D. C.; Schelble, S. M.; Theisen, L. A. *J. Org. Chem.* **1991**, *56*, 1266.
(20) (a) Wiegardt, K.; Bossek, U.; Volckmar, K.; Swiridoff, W.; Weiss, J. *Inorg. Chem.* **1984**, *23*, 1387. (b) Knopp, P.; Wieghardt, K.; Nuber, B.; Weiss, J.; Sheldrick, W. S. *Inorg. Chem.* **1990**, *29*, 363.
(21) Li, X.; Lah, M. S.; Pecoraro, V. L. *Inorg. Chem.* **1988**, *27*, 4657.
(22) (a) Carrano, C. J.; Nunn, C. M.; Quan, R.; Bonadies, J. A.; Pecoraro, V. L. *Inorg. Chem.* **1990**, *29*, 944. (b) Bonadies, J. A.; Butler, W. M.; Pecoraro, V. L.; Carrano, C. J. *Inorg. Chem.* **1987**, *26*, 1218.
(23) (a) Holmes, S.; Carrano, C. J. *Inorg. Chem.* **1991**, *30*, 1231. (b) Kime-Hunt, E.; Spartalian, K.; DeRusha, M.; Nunn, C. M.; Carrano, C. J. *Inorg. Chem.* **1989**, *28*, 4392.
(24) Xioping, L.; Kangjing, Z. *J. Crystallogr. Spectros. Res.* **1986**, *16*, 681.
(25) Cornman, C. R.; Kampf, J.; Pecoraro, V. L. *Inorg. Chem.*, companion paper in this issue.
(26) Prandtl, W.; Hess, L. Z. *Anorg. Chem.* **1913**, *82*, 103.
(27) *International Tables for X-ray Crystallography*; Ibers, J., Hamilton, W., Eds.; Kynoch: Birmingham, England, 1974; Vol. IV, Tables 2.2 and 2.3.1.

Table I. Summary of Crystallographic Data for **1**, **2**, and **3**

	VO(SALIMH)ACAC·CH_3OH (**1**)	VO(SALIMH)SAL·CH_3OH (**2**)	VO(SALIMH)$_2$·$3C_2H_5OH$ (**3**)
formula	$C_{18}H_{23}N_3O_5V_1$	$C_{20}H_{21}N_3O_5V_1$	$C_{30}H_{42}N_6O_6V_1$
mol wt	412.34	434.34	633.64
a, Å	20.673 (4)	12.336 (5)	13.763 (7)
b, Å	21.335 (4)	14.928 (6)	17.589 (4)
c, Å	9.078 (1)	22.03 (1)	14.701 (2)
β, deg	90	90	108.97 (2)
V, Å^3	4404 (1)	4067 (3)	3365 (1)
cryst syst	orthorhombic	orthorhombic	monoclinic
space group	*Pbca*	*Pbca*	$P2_1/c$
d_{calc}, g/cm^3	1.368	1.419	1.251
d_{obs}, g/cm^3	1.38	1.43	1.30
Z	8	8	4
radiation	Mo Kα (0.7107 Å)	Mo Kα (0.7107 Å)	Mo Kα (0.7107 Å)
temperature	ambient	ambient	ambient
abs coeff, mm^{-1}	0.51	0.51	0.33
cryst size, mm	0.28 × 0.50 × 1.0	0.20 × 0.44 × 0.09	0.32 × 0.40 × 0.40
cryst color and habit	red rectangular plate	orange rectangular plate	brown-red cubic fragment
scan speed, deg/min	1.5–15.0	1.5–5.0	2–5
scan range, deg	$0 < 2\theta < 45$	$5 < 2\theta < 50$	$5 < 2\theta < 45$
unique data	2629	3588	4398
no. of obs data	1807 ($F_o > 6\sigma(F)$)	2723 ($F_o > 2.0\sigma(F)$)	3059 ($F_o > 5\sigma(F)$)
octants used	$+h,+k,+l$	$+h,+k,+l$	$+h,+k,\pm l$
	h, 0/9; k, 0/22, l, 0/23	h, 0/15; k, 0/18; l, 0/27	h, 0/15; k, 0/19; l, $\overline{16}$/16
secondary extinction	no correction	12 reflections excluded	10 reflections excluded
residual elect dens, e/Å^3	0.31	+0.88/−0.96	+0.48/−0.48
R^a	0.039	0.0799	0.0697
$R_w{}^b$	0.038	0.0479	0.0949
GOF	1.61	2.52	2.09

$^a R = \sum(|F_o| - |F_c|)/\sum|F_o|$. $^b R_w = [\sum(|F_o| - |F_c|)^2/\sum w|F_o|^2]^{1/2}$.

Table II. Fractional Atomic Coordinates of the Non-Hydrogen Atoms of VO(SALIMH)ACAC (**1**)

atom	x	y	z	U(EQ)^a
V1	0.38033 (3)	0.04749 (3)	0.12402 (7)	0.0377 (2)
O1	0.3723 (1)	−0.0104 (1)	0.0076 (3)	0.047 (1)
O2	0.3228 (1)	0.1110 (1)	0.0335 (3)	0.045 (1)
O3	0.4529 (1)	0.0922 (1)	0.0316 (3)	0.045 (1)
O4	0.3893 (1)	0.1220 (1)	0.2907 (3)	0.047 (1)
N1	0.3079 (2)	0.0185 (2)	0.0623 (4)	0.041 (1)
N2	0.4444 (1)	−0.0022 (2)	0.2602 (4)	0.043 (1)
N3	0.5296 (2)	−0.0555 (2)	0.3204 (4)	0.056 (1)
C1	0.2724 (2)	0.1384 (2)	0.0940 (4)	0.042 (2)
C2	0.2488 (2)	0.1952 (2)	0.0323 (5)	0.056 (2)
C3	0.1959 (2)	0.2245 (2)	0.0881 (6)	0.065 (2)
C4	0.1646 (2)	0.1981 (3)	0.2076 (6)	0.070 (2)
C5	0.1868 (2)	0.1423 (2)	0.2699 (5)	0.058 (2)
C6	0.2407 (2)	0.1114 (2)	0.2164 (4)	0.043 (1)
C7	0.2575 (2)	0.0512 (2)	0.2852 (4)	0.048 (2)
C8	0.3144 (2)	−0.0427 (2)	0.3442 (5)	0.057 (2)
C9	0.3687 (2)	−0.0406 (2)	0.4536 (5)	0.060 (2)
C10	0.4315 (2)	−0.0403 (2)	0.3813 (5)	0.048 (1)
C11	0.5046 (2)	−0.0128 (2)	0.2280 (5)	0.048 (2)
C12	0.4841 (2)	−0.0735 (2)	0.4191 (5)	0.060 (2)
C13	0.5396 (2)	0.1552 (2)	−0.0329 (5)	0.060 (2)
C14	0.4858 (2)	0.1405 (2)	0.0691 (5)	0.042 (1)
C15	0.4747 (2)	0.1785 (2)	0.1909 (5)	0.053 (2)
C16	0.4260 (2)	0.1699 (2)	0.2919 (5)	0.049 (2)
C17	0.4151 (3)	0.2197 (2)	0.4081 (6)	0.087 (2)
O5	0.6478 (2)	−0.1084 (3)	0.2666 (4)	0.115 (2)
C18	0.6935 (2)	−0.1289 (3)	0.3536 (6)	0.099 (3)

$^a U(EQ) = (1/3)\sum_i\sum_j U_{ij}\mathbf{a}_i^*\mathbf{a}_j^*\mathbf{a}_i\cdot\mathbf{a}_j$.

Table III. Fractional Atomic Coordinates for the Non-Hydrogen Atoms of VO(SALIMH)SAL (**2**)

atom	x	y	z	U(EQ)^a
V1	−0.00843 (7)	0.34717 (5)	0.17043 (4)	0.0312 (3)
O1	0.0995 (3)	0.3127 (2)	0.1374 (1)	0.040 (1)
O2	−0.0099 (3)	0.4756 (2)	0.1493 (1)	0.040 (1)
O3	0.0511 (3)	0.3812 (2)	0.2502 (2)	0.035 (1)
N1	−0.1114 (3)	0.3233 (3)	0.0966 (2)	0.035 (2)
N2	−0.0497 (3)	0.2200 (3)	0.2059 (2)	0.036 (2)
N3	−0.0437 (4)	0.0958 (3)	0.2586 (2)	0.051 (2)
C1	−0.0480 (4)	0.5180 (3)	0.1005 (2)	0.034 (2)
C2	−0.0200 (4)	0.6085 (3)	0.0916 (2)	0.041 (2)
C3	−0.0616 (5)	0.6557 (4)	0.0433 (3)	0.051 (2)
C4	−0.1316 (5)	0.6158 (4)	0.0026 (3)	0.054 (2)
C5	−0.1593 (4)	0.5287 (4)	0.0103 (2)	0.045 (2)
C6	−0.1186 (4)	0.4779 (3)	0.0591 (2)	0.032 (2)
C7	−0.1449 (4)	0.3840 (4)	0.0591 (2)	0.038 (2)
C8	−0.1471 (5)	0.2308 (3)	0.0839 (2)	0.051 (2)
C9	−0.2071 (5)	0.1907 (4)	0.1366 (3)	0.054 (2)
C10	−0.1336 (4)	0.1641 (3)	0.1874 (2)	0.038 (2)
C11	0.0030 (5)	0.1753 (3)	0.2488 (2)	0.043 (2)
C12	−0.1298 (4)	0.0878 (4)	0.2205 (2)	0.046 (2)
C13	0.0109 (4)	0.3834 (3)	0.3051 (2)	0.033 (2)
C14	0.0816 (4)	0.3922 (3)	0.3550 (2)	0.038 (2)
C15	0.0437 (5)	0.3968 (4)	0.4130 (3)	0.053 (2)
C16	−0.0672 (5)	0.3935 (4)	0.4252 (3)	0.064 (3)
C17	−0.1379 (5)	0.3847 (4)	0.3783 (3)	0.059 (2)
C18	−0.1019 (4)	0.3815 (3)	0.3175 (2)	0.038 (2)
C19	−0.1817 (4)	0.3811 (3)	0.2703 (3)	0.043 (2)
O4	−0.1654 (3)	0.3774 (2)	0.2152 (2)	0.041 (1)
O5	0.1872 (5)	0.1644 (4)	0.0738 (3)	0.139 (2)
C20	0.2163 (7)	0.1213 (5)	0.1239 (4)	0.155 (4)

$^a U(EQ) = (1/3)\sum_i\sum_j U_{ij}\mathbf{a}_i^*\mathbf{a}_j^*\mathbf{a}_i\cdot\mathbf{a}_j$.

for **2** and 0.086 (5) for **3**). Structure determination summaries are outlined in Table I. Fractional atomic coordinates for **1**–**3** are provided in Tables II–IV.

In **2** the oxygen and carbon atoms (O5 and C20) of the solvent molecule were refined isotropically. All other atoms were allowed to refine anisotropically. Three highly disordered ethanol molecules per vanadium complex were located in the diffraction-quality crystals of **3**. This disorder prevented accurate estimation of the atomic parameters for the ethanol molecules, and constraints were applied to maintain a chemically reasonable geometry. The C_α–O distance was given a starting value of 1.40 Å and allowed to refine as a free variable. The C_α–C_β distance was fixed at 1.069 times the free variable, and the C_β···O distance was fixed at 1.700 times the free variable. Refinement of the geometric constraints[28] converged at values of 1.31 (3) Å for C_α–O and 1.40 (1) Å for C_α–C_β. These values were then allowed to refine as rigid groups with isotropic thermal parameters.

(B) Other Measurements. Electron paramagnetic resonance (EPR) spectra were collected on a Bruker ER 200 instrument at ≈9.47 GHz. DPPH (g = 2.0037) was used as an external standard. Spectra were acquired at 77 K using a quartz finger Dewar. The spectral parameters

(28) Initial values were average values from many ethanol solvates as obtained from the Cambridge crystallographic data base.

Table IV. Fractional Atomic Coordinates for the Non-Hydrogen Atoms of $VO(SALIMH)_2$ (3)

atom	x	y	z	U(EQ)[a]
V1	0.00777 (9)	0.18298 (5)	−0.00482 (7)	0.0479 (4)
O1	0.0935 (4)	0.1332 (2)	0.0731 (3)	0.062 (2)
O2	0.0615 (3)	0.1793 (2)	−0.1138 (3)	0.054 (2)
O3	−0.1040 (3)	0.2546 (2)	−0.0946 (3)	0.052 (2)
N1	−0.0913 (4)	0.0922 (3)	−0.0704 (3)	0.054 (2)
N2	−0.0805 (4)	0.2005 (3)	0.0877 (3)	0.048 (2)
N3	−0.1250 (4)	0.2298 (3)	0.2136 (4)	0.060 (2)
N4	0.0854 (4)	0.2879 (3)	0.0463 (3)	0.053 (2)
N5	0.1823 (4)	0.3055 (3)	−0.1227 (4)	0.062 (2)
N6	0.2842 (6)	0.3943 (4)	−0.1409 (5)	0.088 (3)
C1	0.0794 (5)	0.1163 (3)	−0.1536 (4)	0.055 (3)
C2	0.1664 (6)	0.1117 (4)	−0.1855 (5)	0.063 (3)
C3	0.1838 (6)	0.0459 (4)	−0.2319 (5)	0.073 (3)
C4	0.1161 (8)	−0.0150 (4)	−0.2483 (5)	0.080 (4)
C5	0.0328 (6)	−0.0111 (4)	−0.2165 (5)	0.072 (3)
C6	0.0143 (6)	0.0523 (4)	−0.1681 (4)	0.058 (3)
C7	−0.0723 (5)	0.0478 (4)	−0.1319 (4)	0.060 (3)
C8	−0.1794 (6)	0.0701 (4)	−0.0406 (5)	0.069 (3)
C9	−0.2375 (6)	0.1356 (4)	−0.0189 (5)	0.069 (3)
C10	−0.1795 (5)	0.1762 (4)	0.0714 (4)	0.057 (3)
C11	−0.0504 (6)	0.2334 (3)	0.1750 (4)	0.056 (3)
C12	−0.2081 (6)	0.1943 (4)	0.1500 (5)	0.067 (3)
C13	−0.1343 (5)	0.3205 (3)	−0.0714 (4)	0.050 (2)
C14	−0.2357 (6)	0.3446 (4)	−0.1140 (5)	0.065 (3)
C15	−0.2675 (7)	0.4127 (5)	−0.0925 (6)	0.086 (4)
C16	−0.2030 (8)	0.4620 (5)	−0.0276 (7)	0.089 (4)
C17	−0.1021 (7)	0.4407 (4)	0.0144 (5)	0.074 (4)
C18	−0.0667 (6)	0.3701 (4)	−0.0051 (4)	0.058 (3)
C19	0.0404 (6)	0.3530 (4)	0.0418 (4)	0.055 (3)
C20	0.1958 (6)	0.2856 (4)	0.1026 (4)	0.065 (3)
C21	0.2649 (5)	0.2601 (4)	0.0454 (5)	0.068 (3)
C22	0.2609 (5)	0.3101 (4)	−0.0363 (5)	0.058 (3)
C23	0.2023 (6)	0.3567 (4)	−0.1829 (5)	0.072 (3)
C24	0.3221 (6)	0.3663 (5)	−0.0484 (6)	0.082 (4)
O4	0.342 (1)	0.9771 (8)	0.283 (1)	0.230 (5)
C25	0.302 (1)	0.9182 (8)	0.313 (1)	0.27 (1)
C26	0.379 (1)	0.8782 (8)	0.383 (1)	0.27 (1)
O5	0.408 (1)	0.348 (1)	0.269 (1)	0.261 (6)
C27	0.457 (1)	0.287 (1)	0.310 (1)	0.30 (1)
C28	0.484 (1)	0.292 (1)	0.410 (1)	0.46 (2)
O6	0.474 (2)	−0.021 (1)	0.185 (2)	0.336 (9)
C29	0.441 (2)	0.050 (1)	0.171 (2)	0.54 (3)
C30	0.480 (2)	0.086 (1)	0.105 (2)	0.41 (2)

[a] $U(EQ) = (1/3)\sum_i\sum_j U_{ij}\mathbf{a}_i^*\mathbf{a}_j^*\mathbf{a}_i\cdot\mathbf{a}_j$.

$g_\parallel$, $g_\perp$, $A_\parallel$, and $A_\perp$ were calculated to second order according to Chasteen.[16] Isotropic parameters were calculated as weighted averages of the anisotropic values. UV–vis spectra were recorded on a Perkin-Elmer Lambda 9 instrument. FTIR spectra were collected with a Nicolet 5DX instrument on KBr pellets. Positive and negative FAB mass spectra were acquired by the University of Michigan Mass Spectroscopy facility using 3-nitrobenzyl alcohol as the FAB matrix. Elemental analyses were performed by Galbraith Laboratories, Knoxville, TN.

Results and Discussion

Synthesis. Our synthetic goal was to prepare vanadium compounds containing imidazole both as a coordinated ligand and as an uncoordinated, pendant functional group. Since there is only one report of a vanadium(IV)–imidazole compound in the literature, the formation of additional representatives of this structural type would provide important structural and spectroscopic data necessary for understanding the chemistry of vanadium enzymes. Further, it was anticipated that the coordinated imidazole ligand is acid labile and, therefore, that the coordination site might be accessed under the appropriate reaction conditions. The synthesis of "pendant arm" compounds was of interest since an imidazole group removed from the metal center may act as a general acid/general base catalyst and thus model vanado-enzymes containing ionizable amino acid residues near, but not directly bound to, the metal center. The first goal has been accomplished in all the compounds reported herein. The second goal has been achieved in compound **3**.

Reaction of the ligand HSALIMH, generated by the Schiff base condensation of salicylaldehyde with histamine [4-(2-aminoethyl)imidazole], with various vanadium salts has produced three new complexes which contain imidazole in their coordination sphere as presented in Figure 1. The ligand HSALIMH can be isolated as an oil but is best used in situ immediately after preparation. The preparation of **1** requires a simple ligand-exchange reaction as shown in scheme A of Figure 1. The synthesis of **2** is not as straightforward. Two equivalents of the ligand HSALIMH are required for the reaction while only 1 equiv of $(SALIMH)^-$ is present in the product. Clearly, hydrolysis of the second ligand must be occurring as shown in scheme B of Figure 1. The histamine thus generated is probably necessary to neutralize the acid formed upon deprotonation of the phenolate moieties. The formation of complex **3** from HSALIMH and triethyl vanadate(V), is remarkable for two reasons: First, the $(V^{IV}{=}O)^{2+}$ unit must coordinate two tridentate ligands with only five available coordination sites. Second, the vanadium ion must be reduced from the +5 oxidation state to the +4 oxidation state during the reaction. It should be noted that no tractable products are obtained when only 2 equiv of HSALIMH are used. The extra HSALIMH ligand either is the reducing agent or is required to form a vanadium complex which is then reduced by solvent or an unidentified solution species. This reaction is outlined, in unbalanced form, in scheme C of Figure 1. Studies are in progress to understand completely the mechanism of this reduction which may be of relevence to the site-selective vanadate-sensitized photocleavage of proteins.[29] It is interesting to note that the $(SALIMH)^-$ anion stabilizes vanadium in the +4 oxidation state relative to the +5 oxidation state. This can be contrasted to the ligand *N*-salicylidene-*N*-(2-hydroxyethyl)ethylenediamine (HSHED)[21] and the SALA series of ligands (*N*-(hydroxyalkyl)salicylideneamine)[22a] which form vanadium(IV) complexes that are readily oxidized to vanadium(V) in the presence of oxygen. It has been argued previously that imidazole stabilizes vanadium in the +5 oxidation state and thus the vanadate-induced oxidation of NADH is inhibited in imidazole or histidine buffer.[18,19]

Table V. Important Bond Lengths (Å) and Angles (deg)

	1	2	3
V1–O1	1.635 (3)	1.605 (3)	1.610 (4)
V1–O2	1.981 (3)	1.973 (3)	1.973 (3)
V1–N1	2.054 (3)	2.096 (4)	2.118 (5)
V1–N2	2.099 (3)	2.115 (4)	2.121 (4)
V1–E[a]	1.966 (3)	1.971 (3)	2.143 (5)
V1–A[b]	2.203 (3)	2.223 (3)	2.091 (4)
O1–V1–O2	100.8 (1)	102.3 (3)	100.3 (2)
O1–V1–N1	95.6 (1)	95.7 (2)	97.3 (2)
O1–V1–N2	93.6 (1)	94.6 (2)	93.6 (2)
O1–V1–E	99.7 (1)	100.1 (1)	93.0 (2)
O1–V1–A	176.8 (1)	172.8 (2)	174.3 (1)
O2–V1–N1	91.3 (1)	88.6 (1)	87.8 (2)
O2–V1–N2	165.6 (1)	163.1 (2)	166.1 (2)
O2–V1–E	87.1 (1)	87.9 (1)	92.2 (1)
O2–V1–A	80.9 (1)	84.2 (1)	84.3 (1)
N1–V1–N2	86.9 (1)	89.3 (2)	89.0 (2)
N1–V1–E	164.7 (1)	164.2 (1)	169.5 (2)
N1–V1–A	81.7 (1)	81.3 (1)	86.2 (2)
N2–V1–E	90.9 (1)	89.6 (1)	88.5 (2)
N2–V1–A	84.6 (1)	78.9 (1)	82.0 (1)
E–V1–A	83.0 (1)	83.0 (1)	83.3 (2)

[a] E stands for the heteroatom of the second ligand which is in the equatorial plane. [b] A stands for the heteroatom of the second ligand which is in the axial position trans to the oxo.

Structural Studies. (A) Description of Structures. Compounds **1–3** form an isostructural series of vanadium(IV)–imidazole complexes which maintain the fragment $[V^{IV}(=O)SALIMH]^+$ and vary the bidentate ligand that occupies the fifth and sixth metal coordination sites. Figures 2, 3, and 4 provide ORTEP

(29) (a) Gibbons, I. R.; Mocz, G. In *Vanadium in Biological Systems*; Chasteen, N. D., Ed.; Kluwer Academic Publishers: Dordrecht, The Netherlands, 1990; pp 143–152. (b) Cremo, C. R.; Loo, J. A.; Edmunds, C. G.; Hatlelid, K. M. *Biochemistry* **1992**, *31*, 491.

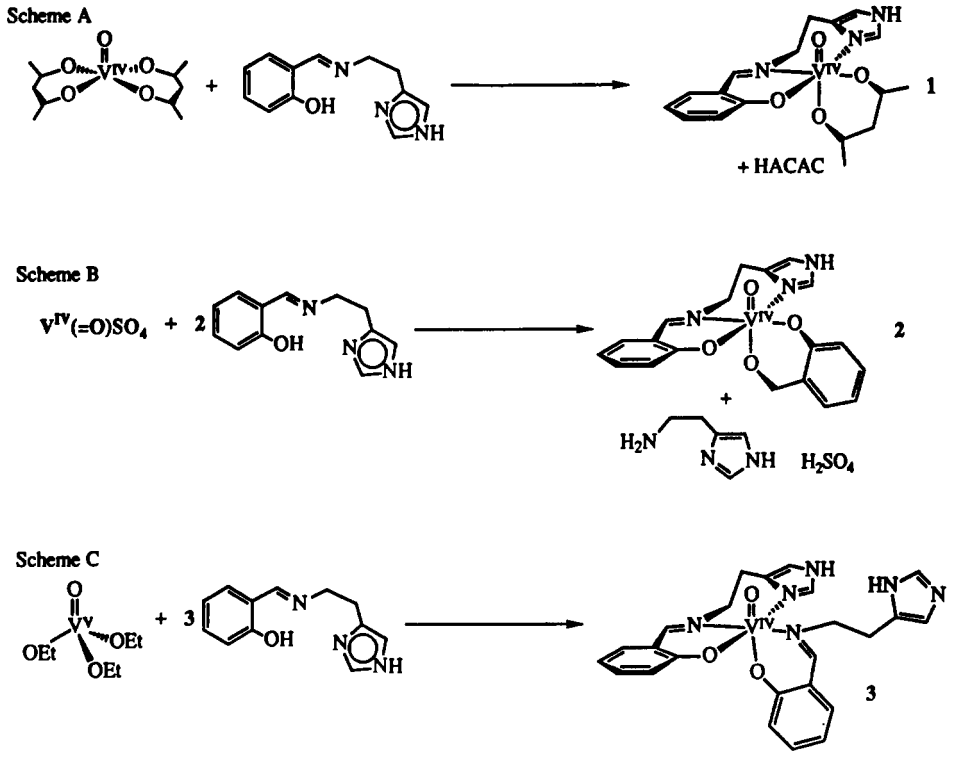

Figure 1. Reaction schemes for the formation of compounds 1–3.

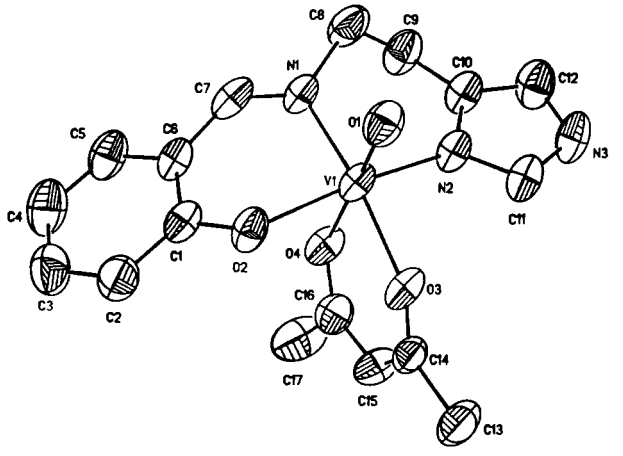

Figure 2. ORTEP diagram of VO(SALIMH)ACAC (1) drawn with thermal ellipsoids at the 50% probability level. Solvent molecules have been omitted for clarity.

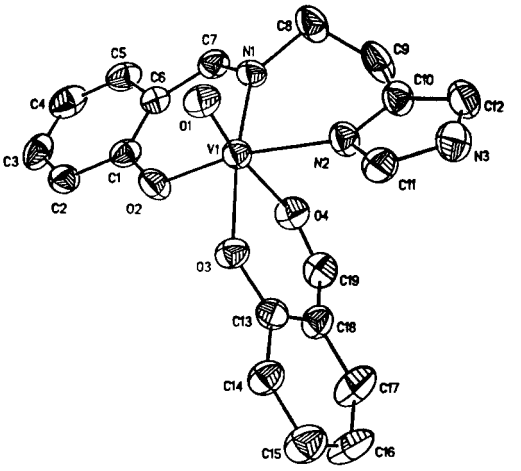

Figure 3. ORTEP diagram of VO(SALIMH)SAL (2) drawn with thermal ellipsoids at the 50% probability level. Solvent molecules have been omitted for clarity.

representations of **1** (ACAC), **2** (SAL), and **3** (SALIMH), respectively. Important bond lengths and angles for these compounds are presented in Table V.

These compounds contain three distinct structural features: the V=O, the $(SALIMH)^-$ ligand, and the exchangeable bidentate chelate. The V=O bond is unexceptional in these materials, falling within the range 1.605–1.635 Å. The vanadium atom is displaced out of the best least squares plane formed by the three donors of $(SALIMH)^-$ and the equatorial donor atom of the bidentate ligand toward the vanadyl oxygen by 0.26, 0.29, and 0.22 Å for **1**, **2**, and **3**, respectively. The $(SALIMH)^-$ is a tridentate meridional ligand that provides phenolate oxygen ($V-O_{av}$ = 1.976 Å), imine nitrogen ($V-N_{av}$ = 2.089 Å), and imidazole nitrogen ($V-N_{av}$ = 2.112 Å) donor atoms to the vanadium(IV). This $V-N_{1m}$ average distance is slightly longer than that observed in $[(CH_3)_4N][V(O)(L\text{-his})(NCS)_2]\cdot H_2O$ ($V-N_{1m}$ = 2.081 (8) Å), which is the only other structurally characterized vanadium(IV)–imidazole complex.[24] These vanadium–imidazole nitrogen distances are similar to the vanadium–imine nitrogen distances of $LV^{IV}(O)Cl(DMF)$ (L = tris(3,5-dimethylpyrazolyl)borate),[23] which are 2.110 and 2.117 Å for the nitrogens cis to the oxo ligand,

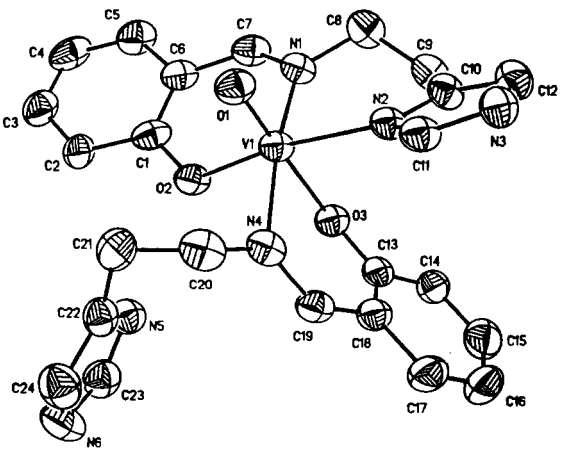

Figure 4. ORTEP diagram of $VO(SALIMH)_2$ (3) drawn with thermal ellipsoids at the 50% probability level. Solvent molecules have been omitted for clarity.

Table VI. EPR Parameters for V-BrPO and Vanadyl Complexes of SALIMH and Other Ligands

compd	g_0	$A_0 \times 10^4$ cm^{-1}	$g_\perp$	$g_\parallel$	$A_\perp \times 10^4$ cm^{-1}	$A_\parallel \times 10^4$ cm^{-1}	ref
V-BrPO, high pH	1.969	87	1.979	1.948	50	160	15
V-BrPO, low pH	1.970	93	1.980	1.950	55	168	15
1/DMF	1.969	92.0	1.977	1.952	56.7	162.7	this work
2/DMF	1.970	91.8	1.979	1.953	56.5	162.3	this work
3/DMF	1.971	90.0	1.979	1.953	55.2	159.6	this work
4/DMF	1.969	94.0	1.977	1.952	57.9	166.4	this work
5/DMF	1.964	101.7	1.976	1.939	64.6	175.9	this work
$VOSO_4$/HCl/DMF	1.963	101.4	1.975	1.940	64.4	175.5	this work
$VOSO_4$/DMF/H_2O, 6 equiv of HCl	1.962	104.8	1.976	1.935	67.2	180.1	this work
2/DMF/H_2O, 0 equiv of HCl(aq)	1.970	90.9	1.978	1.953	55.6	161.7	this work
2/DMF/H_2O, 1 equiv of HCl(aq)	1.969	93.4	1.977	1.953	57.3	165.7	this work
2/DMF/H_2O, 6 equiv of HCl(aq)	1.962	104.9	1.975	1.935	67.2	180.4	this work
{HB(Me_2pz)$_3$VOCl}DMF	1.9854	96					23
{HB(Me_2pz)$_3$VO}ACAC	1.9817	92					23
VO(SHED)	1.968	97	1.979	1.947	64	162	21
VO(HSHED)ACAC	1.971	91	1.982	1.950	60	153	21

while the vanadium–amine nitrogen distances of $(LV^{IV}(O)OH)^+$ (L = triazacyclononane)[20] are slightly longer at 2.151 and 2.159 Å for the equatorial nitrogens. The V–N_{amine} distance in $[(CH_3)_4N][V(O)(L\text{-his})(NCS)_2]\cdot H_2O$ is 2.132 (7) Å.[24] The imidazole plane in compounds **1–3** is not perpendicular to the V=O bond. This is most easily seen in Figure 4 where the dihedral angle between the mean equatorial plane (vida supra) and the mean imidazole plane of **3** is 29 ± 0.4°. For **1** and **2** these angles are 10.7 ± 0.4° and 22.8 ± 0.3°, respectively. In $[(CH_3)_4N][V(O)(L\text{-his})(NCS)_2]\cdot H_2O$ this dihedral angle is 26.3°.[24] While one might expect π interactions between the imidazole and vanadium π-type orbitals to induce a perpendicular orientation between the V=O axis and the mean plane of the imidazole ring, this is clearly not the case, indicating that π-bonding between vanadium and imidazole is not an important feature of the electronic structure in these systems.

A strong trans effect observed in most vanadyl compounds suggests that the weakest donor atom of the variable ligand should be trans to the vanadyl oxygen. This expectation is fulfilled in compounds **1** and **2**, which adopt the predicted structures with long bonds oriented trans to the vanadyl oxygen atom. Although the carbon–carbon and carbon–oxygen distances of the ACAC ligand do not differentiate the ketonic from the enolic oxygen atoms, the similarity of structures **1** and **2** suggests that the neutral carbonyl oxygen is in the axial position. In contrast, **3** has the opposite orientation with the charged phenolate oxygen in the axial position. For this reason, the V–O_{phe} distance (2.09 Å) is intermediate between V–O_{phe} in the equatorial site (av = 1.97 Å) and the neutral oxygen donors in **1** and **2** (2.21 Å). Thus, the trans effect is still expressed when one contrasts the 1.97- and 2.09-Å distances. Interestingly, orientation of the strong phenolate donor trans to the vanadyl oxygen has no effect on the V=O bond distance.

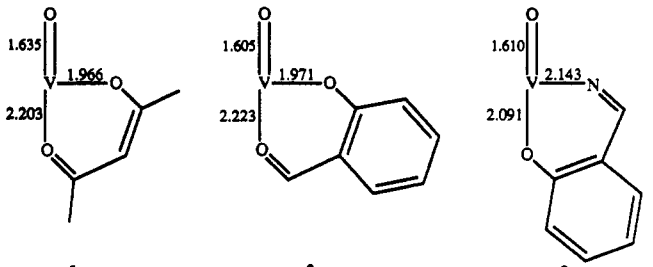

1 **2** **3**

The bidentate $(SALIMH)^-$ could have bonded in two orientations either with the phenolate in the axial position as in Figure 4 or in the equatorial position, which is not observed. These two binding modes define the position of the pendant imidazole relative to the vanadyl oxygen atom. The isolated **3** has the syn configuration of the V=O and imidazole moieties. Thus, the pendant imidazole is positioned ideally to act as an intramolecular acid/base catalyst at the oxo atom.

Compounds **1** and **2** have no short intermolecular distances. The shortest nonbonded distances are between the vanadyl oxo ligand and the lattice solvent (O1–O5, 2.835 and 3.557 Å for **1** and **2**, respectively). Compound **3** has two close interactions. The hydrogen atom attached to N3 (imidazole hydrogen of bound imidazole) is 1.846 Å away from O3 (phenolate oxygen trans to oxo ligand) of a second complex. This distance may indicate an intermolecular hydrogen bond, but it should be noted that this hydrogen was placed at a fixed position (angle C12–N3–H3 = 120°, N3–H3 = 0.96 Å) and thus this distance does not indicate the actual location of the hydrogen atom. O4 (solvent ethanol) is 1.763 Å away from H6 (N_{Im}–H6 of pendant imidazole). Again, it should be noted that this hydrogen is at a fixed position (same constraints as above). The other two solvent molecules may participate in intermolecular hydrogen bonding with each other; however, this is not clear with the disorder problem.

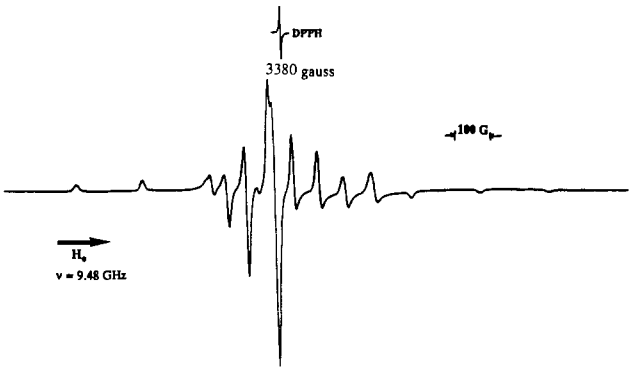

Figure 5. EPR spectrum of VO(SALIMH)ACAC (**1**) in frozen DMF at 77 K. Conditions: acquisition power, 20.2 mW; modulation, 5 GHz; sweep time, 500 s; sweep center, 3500 G; sweep width, 2000 G.

(B) Mass Spectroscopy. Positive and negative FAB mass spectra were collected for compounds **1–3**. Complexes **1** and **2** are characterized by their molecular ion which is the base peak in their negative ion FAB mass spectrum. Compound **3** has a FAB(−) base peak of m/e = 296 ($[VO_2(SALIMH) - H]^-$). Some recombination leads to ions of higher mass than the molecular ion. Positive FAB provided a base peak of m/e = 281 for compounds **1**, **2**, and **3**, which corresponds to the loss of an ACAC, SAL, or SALIMH anion from the molecular ion, respectively. The fragment VO_2SALIM (mass 297) was present in most spectra (mass = 298 for FAB(+) and mass = 296 for FAB(−)).

Solution Studies. (A) EPR Spectroscopy. The EPR spectra of compounds **1–3** are typical of many five- and six-coordinate vanadyl complexes.[16] The spectrum of **1** as a frozen DMF solution, which is representative of all the compounds reported herein, is presented as Figure 5. The axial spectra are characterized by two sets of eight lines which result from coupling of the electron spin to the magnetic moment of the ^{51}V nucleus ($I = {}^7/_2$). Spectral parameters for **1–3** are collected in Table VI. The g and A values are sensitive to the vanadium coordination environment and may be used to distinguish species with different ligation. However, as can be seen in Table VI, **1** and **2** are indistinguishable by EPR spectroscopy in DMF. These two compounds are indeed different

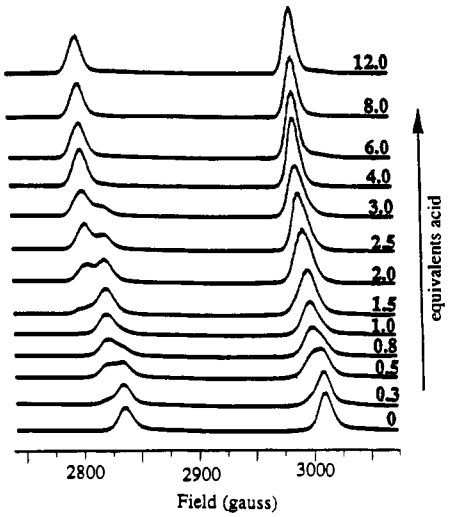

Figure 6. EPR spectra monitoring the acid titration of VO(SALIMH)ACAC (**1**) in frozen DMF at 77 K. Numbers refer to equivalents of acid added. Acquisition parameters were the same as for Figure 5.

in solution as evidenced by visible spectroscopy (vida infra). Compound **3**, on the other hand, is distinct on the basis of a comparison of $A_{\parallel}$, $A_{\perp}$, and A_0 for the three species.

The EPR spectra of **1–3** are sensitive to the presence of acid. Figure 6 presents the data for the titration of **1** (in DMF) with a solution of HCl (anhydrous) in DMF. For evaluation purposes only the two low-field lines ($m = -^7/_2$ and $m = -^5/_2$) of the parallel signal are shown. Two distinct changes are observed between 0 and 4 equiv of acid. Titrimetric addition of 1 equiv of acid (traces 0–1.0 of Figure 6) produces a new species, **4**, which is characterized by a decrease in the resonance field for both low-field resonances. The shift in the $m = -^7/_2$ line is greater than the shift of the $m = -^5/_2$ line, indicating an increase in $A_{\parallel}$ (see Table VI). Addition of a further 3 equiv of acid (traces 1.0–4.0 of Figure 6) results in the formation of a second acid product, **5**, with an even larger $A_{\parallel}$. Subsequent addition of up to 12 equiv of acid produces no change in the parameters g and A. The spectrum of **5** is identical to the spectrum obtained for vanadyl sulfate ($V^{IV}(O)SO_4$) dissolved in acidic DMF as seen in Table VI. The titration data are qualitatively similar for **2** and **3**; however, for **3** 2 equiv of acid is required to complete the first transformation and approximately 6 equiv of acid is necessary for the formation of the second acid product. The protonated forms of all three compounds react stoichiometrically with base to regenerate the starting spectra. It is interesting to note that g_0 (1.970) does not change upon addition of the first proton (second proton for **3**) while A_0 experiences a significant increase from approximately 92 × 10^{-4} to 94 × 10^{-4} cm^{-1}. Upon addition of excess acid (4 equiv for **1** and **2**, 6 equiv for **3**) both g_0 and A_0 experience large changes. g_0 decreases from 1.969 to 1.964, and A_0 increases from 94 to 10^{-4} to 102 × 10^{-4} cm^{-1}. The changes in the isotropic parameters result predominantly from changes in $g_{\parallel}$ and $A_{\parallel}$ as seen in Table VI.

The effect of solvent on the EPR parameters was examined by measuring the spectra on a DMF/H_2O (10/15 v/v) solution of **2**. As seen in Table VI, the parameters for the neutral and monoprotonated species in the binary solvent system exhibit only slight changes from the values found for dry DMF solutions. However, upon addition of excess HCl(aqueous), the anisotropic coupling constants of the solvated vanadyl ion in DMF/H_2O are significantly larger than those found for dry DMF solutions, consistent with the weaker ligand field expected from water coordination.

(B) Electronic Spectroscopy. The electronic spectra of compounds **1–3** are also sensitive to the addition of acid. The spectra for **1–3** in the visible region consist of two or three broad bands of low intensity (ϵ = 30–200 M^{-1} cm^{-1}). The titration of **1** with HCl/DMF is presented in Figure 7. The data indicate three overlapping equilibria. The spectra in plot A show the conversion of **1** to the first protonated species, which is maximized at 0.5 equiv

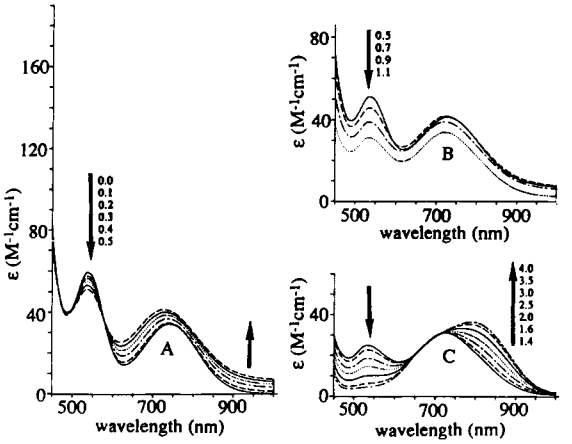

Figure 7. Visible–near-IR spectra following the acid titration of VO(SALIMH)ACAC (**1**) in DMF. Numbers beside arrows refer to equivalents of acid added.

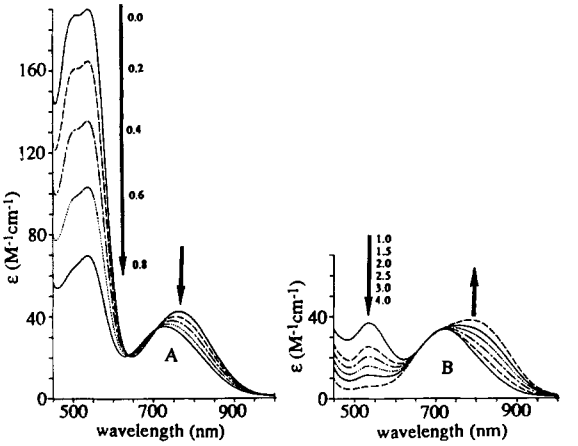

Figure 8. Visible–near-IR spectra following the acid titration of VO(SALIMH)SAL (**2**) in DMF. Numbers beside arrows refer to equivalents of acid added.

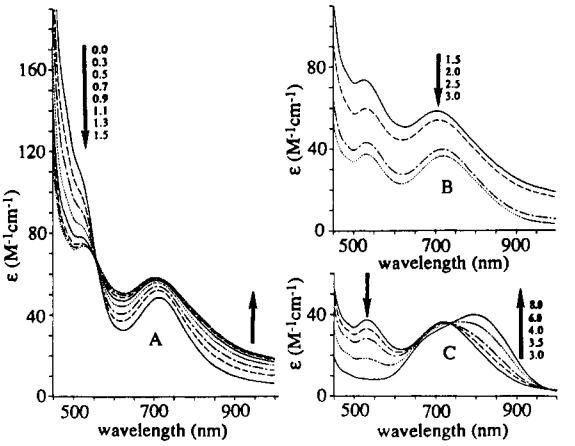

Figure 9. Visible–near-IR spectra following the acid titration of VO(SALIMH)$_2$ (**3**) in DMF. Numbers beside arrows refer to equivalents of acid added.

of acid. In plot B, formation of a second acid-dependent component is indicated by a decrease in absorbance at low energy ($\lambda \approx 730$ nm). Plot C shows the formation of **5** ($\lambda \approx 800$ nm), which is complete after approximately 4 equiv of acid have been added. The titration of **2** is more straightforward as shown in plots A and B of Figure 8. These data are consistent with two consecutive overlapping equilibria, with the first conversion being essentially complete after addition of the first equivalent of acid (plot A). The predominant species in solution at this point in the titration is assigned as **4**, in accordance with the EPR results. The second protonation requires an additional 3 equiv of acid to yield **5** (plot

Scheme I

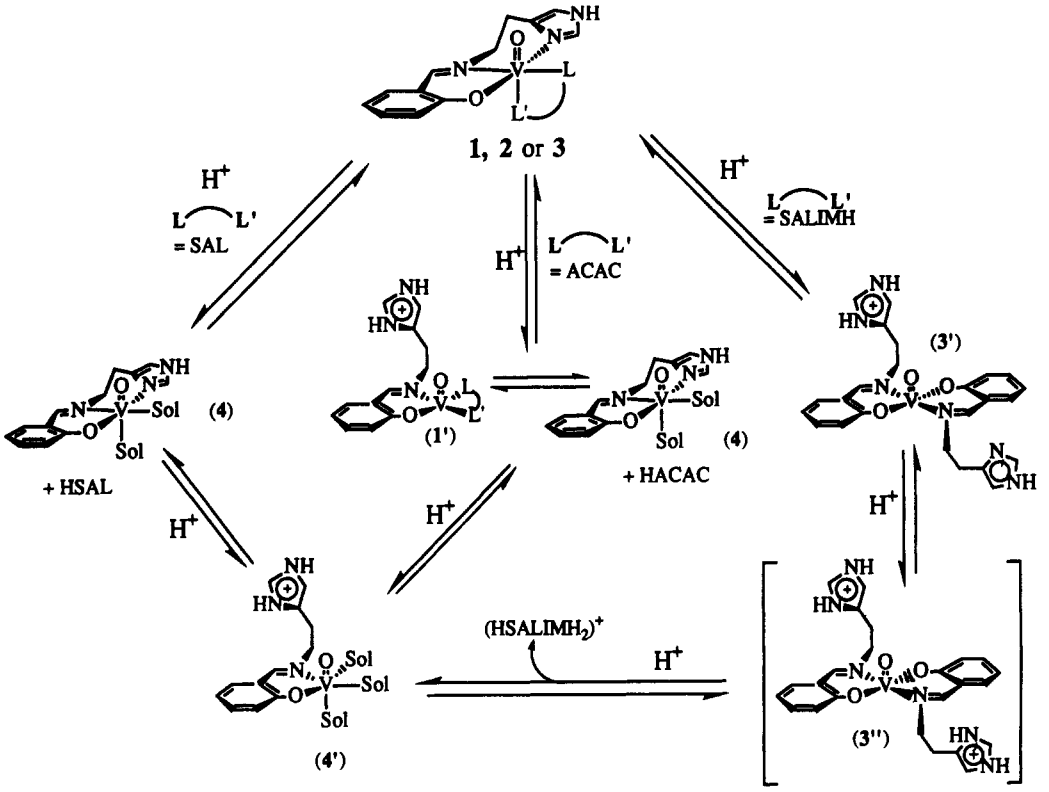

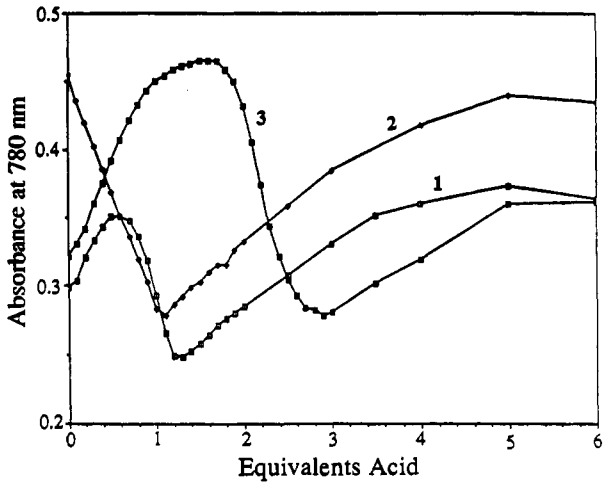

Figure 10. Plot of the absorbance at 780 nm versus equivalents of acid added to DMF solutions of **1**–**3**.

B). Figure 9 presents the data for the titration of **3**. The spectra shown in plots A–C follow the same trends observed for **1** (Figure 7); however, **3** requires more acid to achieve the same spectral changes. An important feature of the spectra of **1** and **3** is the increase in absorbance at low energy (shoulder at approximately 1000 nm) which is not observed during the titration of **2**.

A plot of the absorbance at 780 nm versus equivalents of acid added, provided as Figure 10, clearly shows the different equilibria (changing slopes) for the three titrations. The absorbance value at 780 nm was chosen for the titration profile since in this region the slope of the curve changes sign as opposed to just steepness. At other regions of the spectra, the same conclusions regarding the solution equilibria are reached but the small changes in slope are difficult to observe. The two equilibria observed for **2** may be explained by the protonation and loss of the bidentate ligand to form **4**, which predominates at 1 equiv of acid added, with subsequent protonation and loss of HSALIMH to yield the solvated vanadyl ion, **5**. The absorbance profiles for **1** and **3** have an initial increase in the absorbance and then a decrease to a value

Table VII. Absorbance Maxima (Molar Absorptivity, M^{-1} cm^{-1}) for Different Amounts of Acid Added

compd	0 equiv	1 equiv	2 equiv	3 equiv	excess[a]
1	743 (34)	537 (35)	537 (19)		
	539 (59)	722 (37)	738 (31)	774 (33)	790 (36)
2	537 (210)	536 (41)	536 (23)		
	763 (47)	724 (37)	731 (37)	764 (39)	789 (42)
3			530 (60)	532 (37)	
	713 (49)	706 (58)	708 (54)	720 (36)	793 (40)

[a] 4 equiv for **1** and **2** and 7 equiv for **3**.

consistent with the presence of **4**. This result requires the presence of an observable intermediate during the formation of **4**. After **4** has been formed, additional acid (approximately 1.3 equiv for **1** and 2.9 equiv for **3**) yields spectral changes (decrease in absorbance) which are analogous to those observed for **2**. A decrease in the absorbance after the formation of **5** is believed to result from aerobic oxidation of the solvated vanadyl ion. Upon being allowed to stand overnight, the green solution of **5** (a combination of the blue solvated vanadyl ion and the yellow Schiff base ligand) becomes bright yellow, indicating the oxidation of the metal from the +4 state (blue) to the +5 state (yellow, V_2O_5, or colorless, VO_3^-).

A reaction path consistent with the EPR and visible spectroscopic results is presented as Scheme I. In this scheme, initial protonation occurs at either the bidentate ligand, resulting in solvent displacement to form **4**, or at the bound imidazole group, which leads to formation of the square pyramidal complexes **1′** and **3′**. Compounds **1′**, **3′**, and **4** are indistinguishable by EPR spectroscopy (Table VI) but have distinct visible spectra as indicated in Table VII. At approximately 1 equiv of acid added, **1** and **2** have essentially identical visible spectra while the spectrum of **3** is very different. After the addition of approximately 3 equiv of H^+ to **3**, the visible spectrum is the same as **1** and **2** after the addition of 1 equiv of acid (Table VII and Figures 7–10). Additional protons can then react with **1′** or **3′** to yield **4** (or a protonated version of **4**, i.e., **4′**) via loss of HACAC or HSALIMH. Compound **4′** has been formulated as a vanadyl ion coordinated by three solvent molecules and a bidentate (SALIMH) ligand. Finally, protonation of the remaining bound phenolato

oxygen results in displacement of the cationic $(HSALIMH_2)^+$ ligand by solvent molecules to form **5**.

In compound **3'**, the pendant imidazole can act to buffer the second protonation reaction as shown by the formation of **3''** in Scheme I. This is indeed observed in Figures 9 and 10 between 1.0 and 1.8 equiv of acid added. The shoulder observed at 1000 nm during the titration of **1** and **3** can be attributed to intermediates **1'** and **3'**. This intermediate may remain unobserved during the titration of **2** because of the inability of the SAL ligand to stabilize the square pyramidal structure. Acetylacetonate and imino phenolates are known to form stable square pyramidal vanadyl complexes.[30]

The selectivity of the protonation of **1–3** can be addressed since **1** and **3** form square pyramidal complexes via protonation of the bound imidazole ligand while **2** reacts by protonation of the SAL ligand. It is likely that protonation of the bound imidazole is driven by formation of the stable square pyramidal structures **1'** and **3'**. Structures which cannot adopt a more stable structure upon removal of the imidazole will protonate at the more basic oxyanionic ligand such as ACAC for **1** or SAL for **2**.

Implications for the Structure and Chemistry of Vanadium Bromoperoxidase. The probable structure of the active site in vanadium bromoperoxidase has led to considerable discussion in the literature. On the basis of ^{51}V NMR, which gives a shift of −1250 ppm relative to $VOCl_3$, Rehder et al. have proposed an oxygen-rich coordination environment made up predominantly of carboxylato ligands.[13] This proposal follows from an exhaustive study[14] of the relationships between ligand electronegativity, ligand chelate size, and ^{51}V NMR chemical shift and is consistent with the preponderence of carboxylate residues in the protein. This high-field resonance for the ^{51}V nucleus in the native enzyme has not been modeled by any synthetic compounds to date. The ESEEM data of de Boer and co-workers argue definitively for the presence of nitrogen in the vanadium coordination sphere of the reduced enzyme.[17] EXAFS of the native enzyme suggests the presence a short V=O unit and a slightly longer V–O(N) distance at ≈1.7 Å. In the reduced enzyme, the best fit of the data was achieved with a short oxo distance of 1.6 Å, two or three oxygens/nitrogen donors at 1.96 Å, and two oxygens at 2.05 Å. The structural data reported above for compounds **1–3** are consistent with the EXAFS results for the reduced enzyme. Notably, the 1.98-Å average distance for the vanadium–*cis*-phenolate bond, the 1.62-Å average distance for the vanadium–oxo bond, and the 2.11-Å average distance for the vanadium–imidazole nitrogen bond are very close to the EXAFS values.

The short V–O bond found by EXAFS has precedent in two structurally characterized vanadium compounds: Wieghardt's hydroxy-ligated vanadium–triazacyclononane structure (V–OH = 1.783 Å)[20b] and the vanadium ester structure of Scheidt (V–O–*i*-Pr = 1.774 Å).[31] In structurally characterized compounds, vanadium(V) usually forms the *cis*-dioxo unit VO_2^+ while vanadium(IV) favors the vanadyl $V{=}O^{2+}$ structural motif. Thus, using the carboxylate/vanadate analogy of Floriani, both the acid and the ester are likely candidates for the structure of the metal center.[32] It has been proposed by us[22] and others[23a] that a monooxo–vanadium(V)–phenolate structural unit ($V^V(O)OPh^{2+}$) is unlikely in the native system due to the absence of a LMCT band in the visible spectrum of the enzyme which is always present in synthetic systems. It should be emphasized that this does not rule out the possibility of a dioxo–vanadium(V)–phenolate unit ($V^V(O)_2OPh$) in the native system.

The EPR data for compounds **1–3** show the same trends upon protonation as those observed in reduced V-BrPO; i.e., an increase in acid concentration induces an increase in the vanadium hyperfine coupling constant, A. The results reported for **3** indicate that the protonation of a ionizable residue near, but not attached to, the metal center does not affect the EPR spectra of vanadium(IV) compounds. Thus, we suggest that the changes observed upon decreasing the pH in the reduced native system result from protonation of a bound ligand and not protonation of an unbound residue *near* the metal. Since the effective pK_a's of bound ligands can differ significantly from the pK_a's of unbound ligands, caution should be exercised when metal coordination spheres are assigned on the basis of pK_a's determined from kinetic data. The magnitude of the changes observed upon addition of the first equivalent of acid to **1–3** is smaller than that observed for reduced V-BrPO. The size of the change in the hyperfine coupling constant is dependent on the specific nature of the metal coordination sphere, and thus this work does not distinguish between protonation of a nitrogen or oxygen donor. The presence of an ionizable residue at the active site of the enzyme may be necessary for two reasons: First, protonation of this ligand may be required to open a metal coordination site. Second, the protonated residue may be required for transferring a proton during the activation of peroxide.

Conclusions

Three new members of a novel class of vanadium compounds in which imidazole is coordinated to the metal center have been prepared and characterized both structurally and spectroscopically. These compounds are important since they provide fully characterized models for the structure and spectroscopy of vanadium(IV)–protein interactions. Changes in the EPR and visible spectra of **1–3** upon acidification are consistent with solvent displacement of a protonated ligand. The EPR spectral changes observed upon protonation of **1–3** are similar to those observed for the reduced form of vanadium bromoperoxidase. Acid/base titrations have shown that protonation of either nitrogen or oxygen ligands can yield an increase in the vanadium hyperfine coupling constant and that the residue which is protonated may depend on structural changes at the metal center which are not related to the pK_a of the protonated ligand. These studies have indicated that ligands near the metal center can buffer reactions at the metal center. Continuing studies in our laboratory on these complexes are focusing on the reactivity of the vanadium(V) analogues of the complexes reported above.

Acknowledgment. Financial support from the National Institutes of Health (Grant GM 42703-01A1) is gratefully acknowledged.

Supplementary Material Available: Listings of fractional atomic coordinates, anisotropic thermal parameters, bond lengths and angles, and least squares planes for **1**, **2**, and **3** (24 pages); tables of observed and calculated structure factors for **1**, **2**, and **3** (39 pages). Ordering information is given on any current masthead page.

(30) For example, see bis(acetylacetonato)oxovanadium(IV) (Hon, P. K.; Beford, R. L.; Pfluger, C. E. *J. Chem. Phys.* **1965**, *43*, 3111) and bis[(4-chlorophenyl)salicylideneaminato]oxovanadium(IV) (Pasquali, M.; Marchetti, F.; Floriani, C.; Merlino, S. *J. Chem. Soc., Dalton Trans.* **1977**, 139).

(31) Scheidt, R. W. *Inorg. Chem.* **1973**, *12*, 1758.

(32) Giacomelli, A.; Floriani, C.; De Souza Duarte, A. O.; Chiesi-Villa, A.; Guastini, C. *Inorg. Chem.* **1982**, *21*, 3310.